POLITECNICO DI TORINO
Repository ISTITUZIONALE

Architected 3D-printable hydrogels with amplified piezoionic transduction for self-powered wearables

Original
Architected 3D-printable hydrogels with amplified piezoionic transduction for self-powered wearables / Belduque, M.J.A., Mogli, G., Sacco, A., Roppolo, I., Stassi, S.. - In: CHEMICAL ENGINEERING JOURNAL. - ISSN 1385-8947. - 548:(2026), pp. 1-13. [10.1016/j.cej.2026.182105]

Availability:
This version is available at: 11583/3016228 since: 2026-10-02T08:53:20Z

Publisher:
Elsevier

Published
DOI:10.1016/j.cej.2026.182105

Terms of use:

This article is made available under terms and conditions as specified in the corresponding bibliographic description in the repository

Publisher copyright

(Article begins on next page)

19 November 2026

Chemical Engineering Journal 548 (2026) 182105

Contents lists available at ScienceDirect

Chemical Engineering Journal

journal homepage: www.elsevier.com/locate/cej

Architected 3D-printable hydrogels with amplified piezoionic transduction for self-powered wearables☆

Maria Jose Arias Belduque [a], Giorgio Mogli [a], Adriano Sacco [b], Ignazio Roppolo [a,b], Stefano Stassi [a,*]

[a] Department of Applied Science and Technology, Politecnico di Torino, C.so Duca degli Abruzzi 24, 10129, Turin, Italy
[b] Center for Sustainable Future Technologies @Polito, Istituto Italiano di Tecnologia, Via Livorno, 60, 10144, Turin, Italy

ARTICLE INFO

Keywords:
Piezoionic
Hydrogel
Self-powered device
3D printing
wearable

ABSTRACT

The lack of electronic materials that properly replicate the sensing capabilities of human skin has motivated the search for soft systems that transduce mechanical stimuli through intrinsic physicochemical mechanisms. Piezoionic hydrogels, which under mechanical deformation generate ion flux, offer a promising route toward such functionality. Here we investigate the piezoionic response of a photocurable, self-healing semi-interpenetrating polymer network hydrogel composed of poly(vinyl alcohol), acrylic acid, and poly(ethylene glycol) diacrylate. By systematically varying cation mobility using a series of alkali metal chlorides, we correlate ionic transport with electromechanical output across planar and sandwich electrode configurations under the application of both compressive and tensile mechanical stimuli. Pressure-induced gradients in ionic concentration produce measurable voltage and current outputs when cation and anion mobilities are mismatched, providing a mechanistic analogue to biological mechanoreceptors. We further demonstrate that 3D-printed architecture enhances the piezoionic signal through strain concentration and retain functionality after damage due to the hydrogel's autonomous healing. Finally, we implement these materials as self-powered biometric sensors and mechanical energy harvesters. These results establish a milestone in the design guidelines for ionically driven tactile electronics and highlight that piezoionic materials are cornerstone materials for the next generation of soft robotics, wearable systems, and health-monitoring technologies.

1. Introduction

Tactile sensors are devices capable to interact with a wide range of mechanical stimuli from their surroundings, converting them into electrical signals [1]. They are commonly used to detect and analyze objects according to their physical characteristics such as form and texture [2], which makes them valuable in a wide range of applications such as soft robotics, human-machine interfaces, and health monitoring [3]. In the field of biomedical engineering the research into artificial touch has gained significant momentum, since sensing systems must be designed starting from materials that either resemble or physically interact with soft tissues. This interest has been fueled by the advent of biocompatible devices and the growing demand for sensors that mimic the functionality of human mechanoreceptors. Recent developments, particularly in electronic and artificial skins, aim to replicate the sensory perception and mechanical properties of natural skin. Soft tactile sensors, with their intrinsic flexibility and adaptability, show great promise for these purposes. Nevertheless, despite the rapid advancement of sensory technologies, integrating electronic components with natural materials continues to be difficult. Traditional devices generally demand high power or external energy supplies, exhibit rigid and inflexible architectures, and often show limited repeatability and poor shear resistance [4–6].

Over the years, various operating mechanisms have been explored for tactile sensing, including resistance changes [7,8], capacitance variations [9,10], inductive response to external deformations [11], or friction-based mechanisms between two materials [12,13], among others. In this context, the piezoionic effect is a newly investigated phenomenon in polymeric ionic conductive materials due to its resemblance to ionic transport in several biological processes. When pressure is applied to those materials, ions migrate out of the deformed region, inducing a strain-driven ion flux that generates a net current. If the

☆ This article is part of a Special issue entitled: 'Self-Powered Flexible Electronics' published in Chemical Engineering Journal.

* Corresponding author.
E-mail address: stefano.stassi@polito.it (S. Stassi).

https://doi.org/10.1016/j.cej.2026.182105
Received 1 July 2026; Received in revised form 14 September 2026; Accepted 17 September 2026
Available online 20 September 2026
1385-8947/© 2026 The Authors. Published by Elsevier B.V. This is an open access article under the CC BY license (http://creativecommons.org/licenses/by/4.0/).

mobility of anions and cations differs, their different diffusion within the polymeric matrix will cause a charge imbalance [14,15]. This imbalance is measurable as an electrical voltage in the device, leading to electron movement (current) in the external circuit, both proportional to the applied pressure [16]. Notably, piezoionic sensors are intrinsically self-powered, capable of capturing physiological signals across diverse environments, and operate through ion-transport mechanisms that closely resemble those found in biological cell membranes. These characteristics place piezoionic sensors as ideal candidates for the integration of electronic devices with the human body and the development of biomimetic sensors and energy harvesters [17,18]. However, typical piezoionic sensors mostly rely on planar electrode geometries and mechanical stimuli based on pressure stimuli, while the potential of alternative device architectures and deformation modes have only been explored in a limited number of studies [19], despite their potential to facilitate integration onto various human-related applications.

Due to their similarity with living tissues, hydrogels are the ideal materials for fabricating piezoionic sensors. First, the design of soft tactile sensors requires the use of materials that are flexible, deformable, elastic and lightweighted. Hydrogels are 3D network structures that are characterized by their high-water content, tunable properties, stretchability, and biocompatibility [20]. Thanks to their properties, hydrogels are widely used in biomedical applications [21]. The mobile nature of the polymer networks in hydrogels and the high-water content favor the diffusion of ions throughout the material, allowing electrical responsiveness [20,22]. Moreover, hydrogels can be used in additive manufacturing techniques, also named 3D printing, facilitating the fabrication of structures with complex shapes and high reproducibility, ideals for tactile sensors [23]. Additionally, hydrogels are widely employed in the development of advanced functional materials due to their highly tunable nature and versatility. Through different engineering strategies, their electrical and mechanical properties can be tailored and enhanced to meet the specific requirements of targeted applications. This design flexibility along with their compatibility enables the development of multifunctional materials with improved performance, paving the way for highly innovative and next-generation devices [24,25].

In this work, we investigate the piezoionic effect in photocurable, ionically conductive hydrogels composed of acrylic acid (AAc), poly (vinyl alcohol) (PVA), poly(ethylene glycol diacrylate) (PEGDA), and different chloride salts. In fact, although the design of tactile sensor devices using the piezoionic effect is gaining popularity in a wide range of medical applications, there are still considerable shortcomings that need to be studied. As a recently discovered phenomenon, the lack of research leaves some open questions about the behavior of this mechanism. Most studies focuses on the effect of material properties on the electrical response of piezoionic sensors, however, the influence of the parameters of the mechanical stimulus applied to the material is still under investigation and discussion [26]. Here, these aspects are addressed by a systematic investigation of the piezoionic effect under different mechanical stimuli and device configurations. The hydrogels demonstrate the ability to generate electrical voltage and current not only under compressive stress, as commonly reported, but also under tensile strain, thereby extending its applicability for detecting a wider range of mechanical stimuli. In addition, both parallel and sandwich-like electrodes configurations are investigated, exploring the influence of device design on the generated electrical response. The material also exhibits spontaneous self-healing, with recovery of piezoionic performance after damage. Furthermore the influence of ionic species mobility on electrical output was systematically characterized by varying the cations in the chloride salts. Beyond material and device design, the photocurable hydrogels were processed via light induced 3D printing to fabricate complex architectures, demonstrating that, thanks to a geometrical amplification of the mechanical stress concentration, the piezoionic output can be enhanced of an order of magnitude. Finally, the 3D-printed hydrogels were successfully integrated into self-powered biometric sensors for physiological signal monitoring and into piezoionic hydrogel nanogenerators (PHNGs) for energy storage (Fig. 1a). These results highlight the potential of photocurable ionic hydrogels as versatile platforms for soft tactile sensing, wearable electronics, health monitoring, and energy harvesting applications.

2. Results and discussion

2.1. Piezoionic hydrogel materials

The hydrogel developed in this work is based on a polymeric network formed via radical induced photopolymerization between AAc and PEGDA, interpenetrated with a physical network of PVA, and contains over 60% of water. This material, reported in previous studies, was developed for vat photopolymerization 3D printing technologies and enables efficient self-healing without external triggers due to the capability of PVA to form entanglements and H-bonds with polar groups [27,28]. The ionic conductivity is achieved by adding chloride salts with cations of different sizes to the mixture to demonstrate the importance of different ions mobility in the piezoionic phenomenon which is dependent on the size of the hydrated ions in the hydrogel and the interaction with the complex polymeric network, as will be described later. In particular, the alkali series of cations (Li^+, Na^+, K^+, Rb^+) was followed. The hydrogel formulation process is presented in Fig. 1b and is explained in detail in the Materials and Methods section. Before analyzing the geometry role in the piezoionic effect, different simple flat devices were fabricated via 3D printing to assess the hydrogel electrical response to a wide range of physical stimulus (Fig. 1c) and to deeply investigate the phenomenon.

First evidence of the appearance of piezoionic phenomenon was tested in specimens in parallel configuration containing lithium chloride (LiCl). Thin strip copper electrodes placed 15 mm apart were used to collect the signals that were obtained locally applying pressure along 5 different points of the specimen via continuous deformations. The electrical output current to the different touches in each sensor zone is presented in Fig. 1d and e. Once the mechanical stimulus is applied, a response is obtained from the sensor, demonstrating that it is possible to generate an electrical response only with the mechanical deformation of the material, showing the possibility to work as a potential self-powered sensor [14,29]. It is also evident the correlation between the intensity and the polarity of the electrical response and the position of the applied stimulus, which is a typical fingerprint of piezoionic phenomenon [14,30]. In the hydrogel we expect that Li^+ has a mobility lower than that of Cl^- due to its larger hydrated ion diameter, and to its interaction with the nucleophilic moieties of the polymeric network [31,32]. In details, the mechanical stimulus expels Cl^- anions out of the compressed area, causing an intense potential difference due to a local higher concentration of Li^+ cations, generating an overall current dominated by the anion movement [14,33]. Near the center of the sensor (Z3), the signal tends to be smaller as ions are expected to move equally in opposite directions from the deformed region, balancing the effect above mentioned. But when the stimulus is applied on the electrodes (E1 and E2) or very close to them (Z2 and Z3), the current is higher, and it has a more defined shape. Consequently, it is also possible to determine the position in which the pressure has been applied. As shown in Fig. 1e, when pressure is applied around the negative electrode (E1), a positive current is generated because the movement of anions toward the negative electrode (E2) dominates over that of the cations. As the mechanical stimulus moves toward the centre (position Z2, Z3 and Z4), the current decreases toward zero and then becomes negative when the compression is close to the positive electrode. Finally, pressing over the positive electrode (E2) ion migration occurs toward the negative electrode, although the overall response remains primarily governed by anion motion, resulting in a negative current [30]. Therefore, it is evident that the direction of the current depends on both the location of the perturbation relative to each electrode and the mobility of the

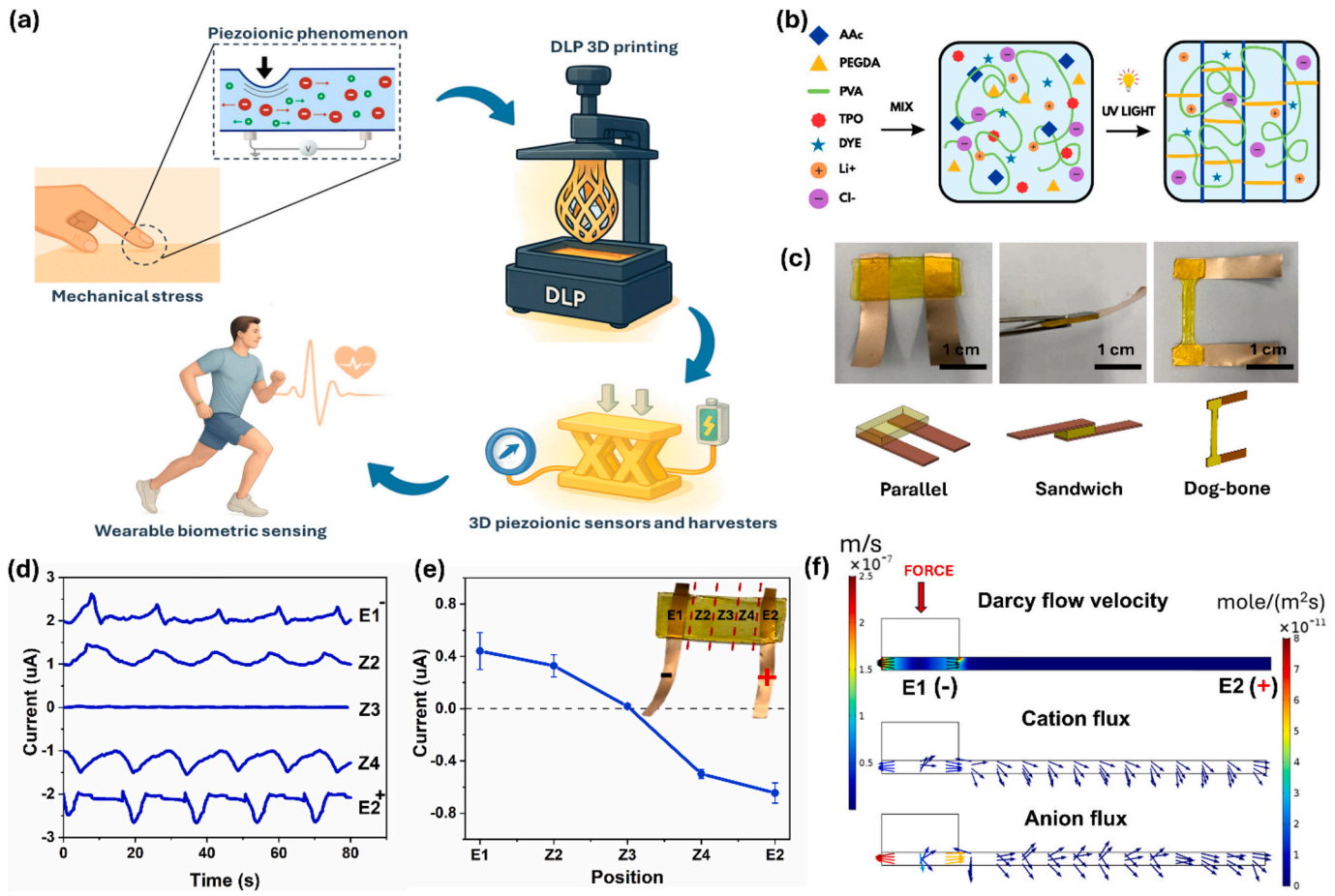


Fig. 1. Photocurable conductive hydrogel synthesis and piezoionic mechanisms. a) Schematic illustration of the exploitation of piezoionic phenomenon for fabricating 3D printed self-powered biometric sensors or energy harvesters. In the top of the image is represented the piezoionic effect in a polymeric material subjected to an external mechanical stimulus that produces an ionic displacement away from the deformation region and an ion flux measurable as an electrical response. b) Schematic of the preparation process of the ionic conductive hydrogel with a semi-interpenetrated network in an aqueous solution. c) Photopolymerized hydrogel flat samples with polyimide copper electrodes positioned in different configurations (parallel, sandwich and dog-bone) with their respective STL models. d) Current response of the hydrogel parallel sample to continuous deformations in 5 different zones of the device (curves were vertically shifted for clarity). e) Change in the polarity of the current output peaks according to the position of the stimulus. The inset shows the type of sample used during the test and the areas where the stimuli were applied. f) Simulated Darcy flow velocity (scale bar on the left) and related cation and anion fluxes (same scale bar on the right) in the hydrogel parallel sample shown in e) under the application of a force over the first electrode area (E1).

different ionic species. Copper-based electrodes were used to record the electrical responses of the samples. A comparison between piezoionic hydrogels interfaced with metallic and carbon-based electrodes was conducted under identical conditions to assess the influence of contact electrification and electric double layer (EDL) effects. The measured voltage and current outputs exhibit comparable values across the different electrodes, indicating that the observed signal is predominantly governed by piezoionic phenomena (Fig. S1). Furthermore, the relatively slow response to mechanical stimulation, together with the absence of an opposite polarity peak upon pressure release, supports the piezoionic origin of the signal and suggests that triboelectric contributions are negligible.

Piezoionic observations can be theoretically described by a model that combines poroelastic Darcy flow with the Poisson–Nernst–Planck (PNP) framework, as previously proposed [16,34]. Hydrogels can be considered as a two-phase system, consisting of an aqueous electrolyte (water with dissolved salts) permeating a polymeric network with free space. When a pressure gradient ∇p is applied to the hydrogel, the solvent is driven away from the deformed region with a mass-averaged velocity u governed by Darcy's law:

$$\boldsymbol{u} = \frac{\kappa}{\mu}\nabla p \tag{1}$$

where κ is the permeability of the gel and μ is the solvent viscosity. This solvent flow induces an initial ionic current, comprising both cations and anions, through convective transport of the electrolyte. The resulting charge movement produces ion concentration and potential gradients that generate diffusive and electrophoretic fluxes opposing the convective flow. The total flux of each ionic species is described by the PNP equation, which accounts for convection, diffusion, and migration:

$$\frac{\partial c_i}{\partial t} = \boldsymbol{u}c_i - D_i\nabla c_i - z_i c_i \mu_i \nabla V \tag{2}$$

where c_i is concentration of the ionic species i (cation or anion) in the solvent, D_i is diffusion coefficient, z_i is valence charge, μ_i is the electrophoretic mobility.

In a purely poroelastic flow, all solute molecules are convected at the same velocity as the solvent, resulting in identical cationic and anionic transport and, consequently, no net current or potential difference should be observed. In contrast, the piezoionic effect assumes a molecular flow regime, in which ions move at different effective velocities relative to the solvent. In this regime, the poroelastic flow preferentially entrains the more diffusive ionic species at a higher rate than counterions with lower diffusivity. To account for this effect, the convective term is modified by scaling the velocity of each species induced by

solvent speed by its diffusion coefficient divided by the ratio of the cationic and anionic diffusivity $\boldsymbol{u}(D_i/(D_+ + D_-))$. Since the diffusion coefficient reflects the degree of hindrance to ionic motion, arising from steric and electrostatic interactions, it serves as a measure of how strongly each species couples to the flow. The differences in ionic diffusivity led to asymmetric redistribution of ions under mechanical perturbation, producing a non-uniform ionic charge distribution. This imbalance generates both diffusive backflow toward chemical equilibrium and electrophoretic migration. The resulting disparity in cationic and anionic fluxes creates a non-neutral local space charge density ρ, which in turn induces an electric potential distribution V within the hydrogel, governed by Poisson's equation:

$$\nabla^2 V = \frac{\rho}{\varepsilon} \tag{3}$$

where ε is the permittivity of medium.

To correlate the theoretical framework with our experimental findings, a simulation model was developed that integrates the previously described equations. The model reproduces a piezoionic hydrogel in a parallel-electrode configuration, with dimensions matching those in Fig. 1c. Fig. 1f illustrates the effect of applying pressure near the first (negative) electrode (E1). The applied force induces solution motion within the porous medium, computed according to Darcy's law. The resulting Darcy flow velocity is concentrated along the boundary of the compressed region, pushing the solution and ions toward the second electrode. Due to the difference in ionic mobilities, the compression generates both cation (Li^+) and anion (Cl^-) fluxes of similar spatial distribution, though the anion flux is several times greater in magnitude. This imbalance drives a net movement of negative ions toward the positive electrode, resulting in a positive current. Conversely, when pressure is applied near the positive electrode (E2) (Fig. S2), the current reverses polarity. When the force is applied at the center, the cation and anion fluxes remain distinct in magnitude but are symmetrically distributed, leading to an overall zero net current (Fig. S3). The effective ionic mobility values used in the simulations were derived from electrochemical impedance spectroscopy (EIS) measurements, as discussed later in this work. Their orders of magnitude are consistent with those reported for comparable systems in the literature [32,34], while the observed variations can be attributed to differences in polymer-matrix composition, network structure, and ion–polymer interactions. Further

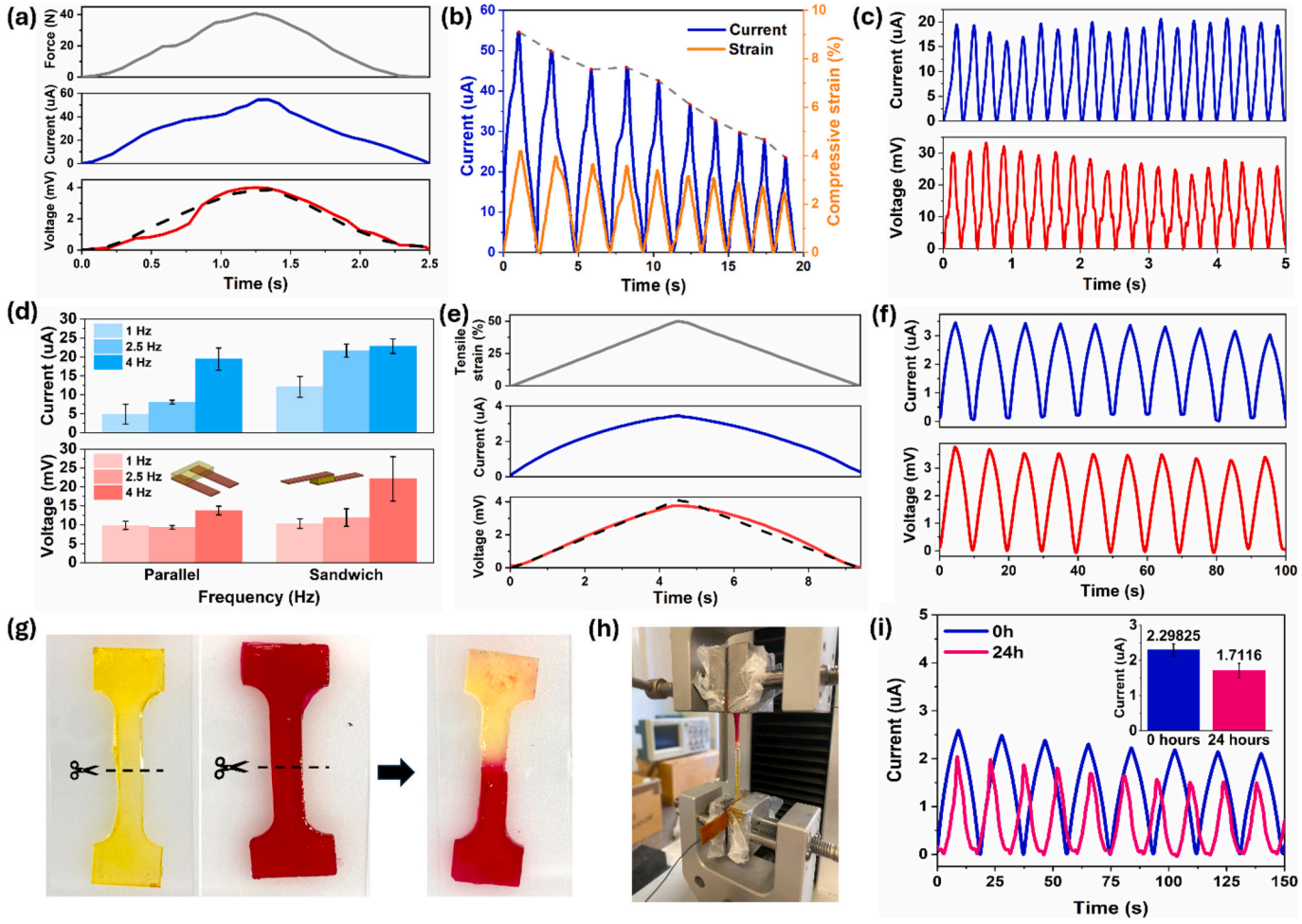


Fig. 2. Mechanical and electrical characterization of a PVA/AAc/LiCl piezoionic sensor. a) Electrical current (middle) and voltage (bottom) responses of a sandwich-shaped sample to an external stimulus of 40 N (top). Simulated voltage response is superimposed with a dashed line to the experimental data. b) Current and strain behavior during a cyclic compression stimulus of 40 N at 25 mm min^{-1} in a sandwich-shaped sample. The dotted line follows the decay of the current for each cycle. c) Electrical current and voltage output of sandwich sample to a constant mechanical pressure of 10 N at 4 Hz. d) Comparison of the electrical outputs of current and voltage to mechanical pressure for both samples in sandwich and parallel configurations, at different frequencies and a constant force (10N). Error bars represent the standard deviation of peak values over 10 consecutive cycles. e) Electrical current (middle) and voltage (bottom) responses of a dog-bone sample to a tensile test with a strain from 0% to 50% (top). Simulated voltage response is superimposed with a dashed line to the experimental data. f) Electrical current and voltage output of a dog-bone sample subjected to a cyclic tensile test (at a speed of 200 mm min^{-1} in the range 0–50% of strain). g) Pristine tensile test specimens (left) and self-healed sample after 24 h (right). h) Self-healed sample subjected to a cyclic tensile test. i) Current output variation of pristine and self-healed samples subjected to a cyclic tensile test (strain range of 0–50% and speed of 200 mm min^{-1}). The inset shows the bar graph with the average current value of 10 consecutive cycles.

details on the simulation model and parameters are reported in the Experimental section and in the Supporting Information.

Once the piezoionic phenomenon was recognized in the hydrogel, further electro-mechanical tests were carried out to fully characterize the phenomenon. Before proceeding with 3D structuration, characterizations were performed on flat specimens (Fig. 1c) to evaluate the material piezoionic performances. Fig. 2a shows the typical behavior of a piezoionic sandwich sample under mechanical stimulation. The "sandwich" electrode configuration is innovative for piezoionic materials, since previous studies have focused exclusively on parallel electrode arrangements [16,30,34,35]. Evaluating the piezoionic output in this configuration is particularly important because it closely reflects the most commonly employed setups in tactile sensing and energy harvesting applications, such as piezoelectric and triboelectric nanogenerators [36,37]. The generated output voltage has been simulated with the model presented before and well describe the experimental result (dashed line in Fig. 2a). The voltage output is generated from the difference in cation and anion flux, where chloride ions move faster than lithium ones in the polymeric matrix, resulting in areas of the specimen with a predominance of negative charges (Fig. S4, Supporting Information). Current and voltage outputs start to grow in accordance with the ionic flow until the load is released, then the hydrogel begins to recover from the deformation, and the electrical response decreases as the gradient concentration drops, until equilibrium is reached or until another stimulation is applied, demonstrating a transient piezoionic effect [26]. Cyclic test was also performed applying 10 cycles at a maximum force of 40 N and speed of 25 mm min^{-1}. Prolonged deformations limit the sample's mechanical relaxation period, resulting in a reduced electrical outcome compared to the beginning of the test. In particular, each deformation cycle leads to material stiffening and a nonlinear stress-strain response, as confirmed in Fig. S5. This is a consequence of the viscoelastic behavior of hydrogels, which does not recover immediately the deformation after each perturbation (Fig. 2b), differently than purely elastic materials [38]. This effect is common in viscoelastic materials, such as elastomers and gels. However, it does not preclude their application in wearable devices or robotics, since hysteresis and other nonlinearities can be compensated for using relatively simple calibration algorithms or, for more complex responses, data-driven approaches based on machine learning and artificial neural networks [39–41]. Furthermore, under repeated loading, the initially pronounced stress-softening and hysteretic response often approaches a stabilized or repeatable state after a limited number of conditioning cycles, further facilitating calibration and compensation in practical applications. To evaluate the hydrogel's functional stability, an electrical recovery test was conducted following continuous cyclic compression with rest time intervals (0 min, 2 min, 5 min and 10 min) between each cyclic stimulus. The aim was to confirm that the material's viscoelastic behavior correlates to a temporary response that is reversible and able to recover overtime rather than permanent functional fatigue, results are shown in Fig. S6. The temporal evaporation of water signifies another prevalent constraint of hydrogel materials, as the loss of water can alter the internal structure of the polymer matrix, ultimately compromising their electrical properties, this led to a gradual loss of functionality, which is a critical concern for applications requiring long-term and reliable performance, particularly in wearable devices and soft-sensing systems. An alternative approach to overcome this limitation is to exploit the intrinsic properties of the material itself. In this case, the hydrogel's ability to rehydrate after drying can be leveraged as a strategy to restore its water content and, consequently, recover its functional electrical performance (Fig. S7). In addition, this hydrogel long-term stability has been demonstrated before [28], with the material recovering its properties after prolongated storage conditions.

An electromechanical actuator (shaker) was used to perform a dynamic mechanical analysis at various frequencies and stresses in order to investigate the material's behavior in a continuously vibrating environment, simulating prolonged and periodically mechanical deformations. Both samples in parallel and sandwich configuration were subjected to cyclic mechanical deformations with a force of 10 N at frequencies of 1 Hz, 2.5 Hz and 4 Hz. The results of the piezoionic voltage and current waveforms obtained with a sandwich specimen are shown in Fig. 2c. At a pressure of 66.67 kPa, the sensor achieves current and voltage values of approximately 20 μA and 30 mV respectively, which are comparable or higher than other performing piezoionic sensors in the literature [4,15,34]. In contrast to slower cyclic compression tests, high-speed mechanical perturbations induce a more elastic response, with lower deformation [42]. On the other hand, the device maintains a rapid and stable electrical response, indicating that the signal generation is directly correlated to the stimuli network response, and therefore could be designed and predicted according to the hydrogel's characteristics [43]. Higher frequencies lead to increased current and voltage readings, furthermore, sandwich configuration generated higher electrical voltage and current, indicating that the proximity of the electrodes intensifies the response (Fig. 2d). It can be observed that a constant deformation (as the case of elastic deformation at high frequencies) creates a higher pressure gradient and stronger potential differences, that cannot be compensated by the fluid flow within the polymer as the case of slow deformation [26]. Additionally, when the electrodes are positioned further apart, the electrical response is reduced because the ions must travel longer distances and can dissipate their kinetic energy more easily [44]. Closer electrodes cause a lower resistance to ionic flow and a more intense and concentrated electric field.

In our work, we also investigated the phenomenon under tensile stress, where material stretching occurs, thereby demonstrating the applicability of piezoionic materials for strain sensing. As seen in Fig. 2e, when the hydrogel is stretched, an immediate electrical current and voltage response like the one obtained with mechanical compression is produced. We attribute the piezoionic output generated under tensile strain to the lateral squeeze of the hydrogel, its contraction along the axis perpendicular to the applied deformation due to the Poisson effect. This transverse compression generates a local pressure gradient that drives ionic redistribution within the deformed region. As in the compression experiments, Cl^- ions migrate more rapidly than Li^+ ions, producing a transient charge imbalance and, consequently, an electrical signal. The intensity of the electrical values that can be achieved by stretching vertically the material is lower compared to a compressive deformation. According to the previous observations, this effect may be related to the increase of the distance between the electrodes due to the material's stretching, therefore increasing the ions conduction path. The tensile study was carried out at different stretching rates to validate the proposed mechanism (Fig. S8). At the lowest tensile rate investigated (1 mm min^{-1}), ionic redistribution can keep pace with the applied deformation, allowing the system to remain close to electrochemical equilibrium (Fig. S9). Consequently, no appreciable transient charge imbalance develops between the cations and anions, and the resulting piezoionic signal is negligible. Increasing the deformation rate, higher piezoionic current and voltage are obtained up to a speed of 200 mm min^{-1}. At higher speeds, the piezoionic signal reaches saturation, likely due to the limited ion mobility within the hydrogel matrix of the ion species compared to the rate of the mechanical stimulus which is too fast to create a further increase in charge imbalance. This result is in good agreement with the previous observations related to the viscoelastic behavior of the network. Again, the piezoionic response of the hydrogel under cyclic tensile loading (50% strain, 200 mm min^{-1}) is shown in Fig. 2f, revealing a highly reproducible signal.

An additional feature investigated takes advantage of the self-healing properties of the hydrogel employed. Flexible sensor devices need to enable continuous electrical recording and to act similarly to some biological tissues, e.g. skin. Therefore, the possibility to work after damages is crucial. Noteworthy, while the recovery of mechanical properties after cutting, enabled by self-healing capabilities, has been widely demonstrated in hydrogel materials [45], the restoration of the piezoionic effect is not very common. Two dumbbell shape specimens

were employed to test this property. These samples were cut into two halves, and then the counterparts were joined together. To clearly observe the repair between the extremities in one of the specimens, tartrazine dye was used (yellow color) while in the other one methyl red dye (red color) was employed, as shown in Fig. 2g. The mending mechanism in these systems is well explained in literature and it is related to both reversible hydrogen bonds formed and the interdiffusion ability of PVA chains [27,28,46]. After 24 h of repair, the self-healed samples were subjected to a cyclic tensile test (Fig. 2h) to evaluate the electrical current output before and after cutting. As can be seen in Fig. 2i, the piezoionic response recovers 80% of the value before the cut. Regarding mechanical properties, the healed specimens follow the behavior of the original specimen in the 0–50% strain range investigated for piezoionic analysis, and the Young's modules remain comparable (Fig. S10). The slight reduction in mechanical properties may be attributed to the not completely uniform repair of the polymer network, so that not all bonds are restored, which could also have impacted on the electrical generated output. Preserve the piezoionic behavior opens a new perspective for this class of materials for advanced electronic applications, in particular biomimetic.

2.2. *Effect of ionic mobility on piezoionic output*

As previously stated, the electrical output acquired from a piezoionic sensor is due to the separation of anions and cations in response to an external mechanical deformation. Consequently, if the ionic mobilities between the species within the material differs, the pressure gradient generated will be greater, and therefore the electrical responses will be higher [34]. Therefore, the influence of the ionic mobility of different species added to the polymeric matrix was experimentally studied using different chloride salts (LiCl, NaCl, KCl and RbCl), in order to keep a fixed anion (Cl^-) as reference while varying only the cation, following

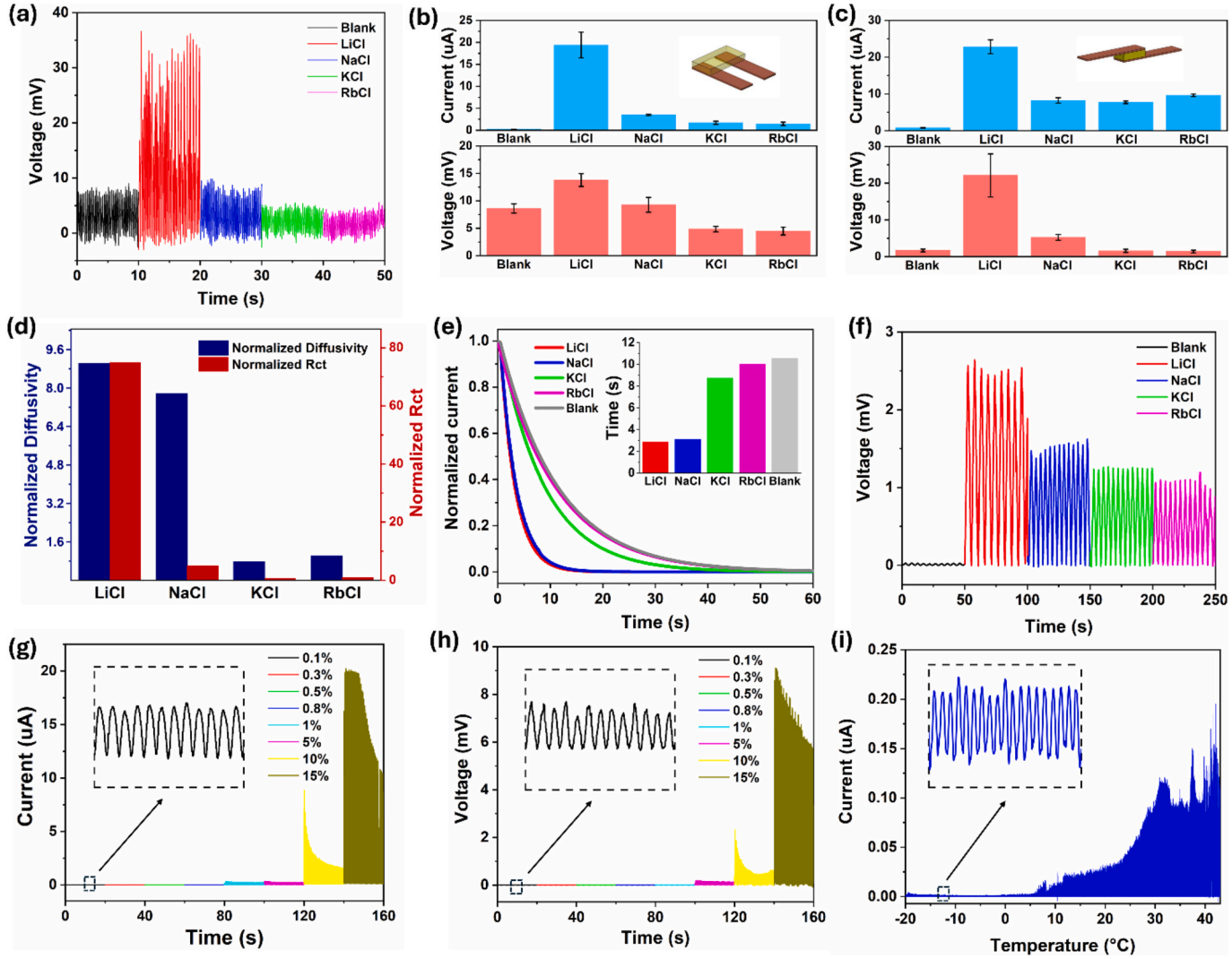


Fig. 3. Analysis of ionic conductivity in different PVA/AAc samples and electrical response under different parameters. a) Electrical voltage output of sandwich samples containing different salts to a constant local pressure of 10 N at 4 Hz. Comparison of the electrical outputs of current and voltage to a mechanical deformation for samples in b) parallel and c) sandwich configurations (frequency of 4 Hz and a constant force of 10 N). Error bars represent the standard deviation of peak values over 10 consecutive cycles. d) Diffusivity and charge transfer resistance values for each of the salts obtained during EIS test on a parallel sample. The values of the diffusivity and the charge transfer resistance were normalized with respect to the ones of RbCl sample. e) Current stabilization over time according to the salt content within a sandwich sample after a constant force deformation (80 N). Inset shows the bar chart with the time value for each of the salts. f) Voltage responses of dog-bone samples containing different salts, subjected to a cyclic tensile test at a speed of 200 mm min^{-1} in the range 0–20% of strain. g) Electrical current and h) voltage output of a PVA/AAc/LiCl sample (1.5 × 15 × 10 mm^3) to a dynamic analysis under small compressive deformations (range from 0.1% to 15% strain). Insets illustrate a zoom of the cycles of some electrical cyclic responses. i) Current output to a dynamic mechanical thermal test at 1 Hz and 1% strain deformation in compression setup (temperature range from −20 °C to 43 °C).

the alkali series. The impact of the different cation was evaluated stimulating the different hydrogels under the same mechanical stress profile. Consequently, preliminary studies were carried out to evaluate the potential impact of each salt on certain mechanical properties of the material. First, the rheology of the precursor ink was investigated to recognize changes in viscosity. Fig. S11 shows the results obtained for the resins with different salt types and without added salt (blank). It is possible to observe an increase in viscosity in the presence of salts, especially with those containing larger cations due to a modification of intramolecular interactions. Similarly, the Young's Modulus of all samples were analyzed. The addition of salt causes the material to become slightly more rigid following the alkali series, in good agreement with the behavior of other hydrogels reported in literature [47–50] (Fig. S12 and Table S1). However, the values remain within a narrow range between 70 kPa and 120 kPa, indicating comparable mechanical properties.

The voltage output signal obtained under a compression test performed at peak load of 10 N and 4 Hz using the mechanical shaker on sandwich samples is reported in Fig. 3a. The highest values measured were obtained with the LiCl and the output progressively decreased with increasing salt molecular weight. Current output shows a similar behavior, even with the different electrode configuration and lower frequency (Fig. S13). Fig. 3b and c shows the peak voltage and current outputs obtained with cyclic compressive load on the parallel and sandwich configurations, respectively. In both cases, the highest response is obtained with LiCl and as demonstrated before, the values are higher when the electrodes are closer (sandwich configuration). This behavior was expected from the theoretical description of the piezoionic phenomenon. In fact, as widely reported in literature, the metal of alkali series follow a clear trend in ionic mobility in ionic hydrogels ($Rb^+ > K^+ > Na^+ > Li^+$) while the mobility of counterion is barely affected [51]. This is due to the interaction of cations with the polymeric macromolecules. Therefore it can be stated that Li cations have reduced mobility under mechanical stress, while Cl anions maintain their diffusivity, causing higher charge separation. It must be noted that the electrical response of the reference (blank) is different from zero because the carboxylic groups present in the acrylic acid dissociate in water, and therefore protons remain free and mobile within the material, even if their concentration is much lower with respect to the ions present in the sample prepared with chlorine salts. To confirm the previous results, an EIS analysis was carried out on the different hydrogels to deeply analyze their electrical properties. The impedance signals were fitted using a model of an experimental circuit (see Fig. S14). The test was conducted using parallel-configured sensors, with tiny electrodes spaced 10 μm apart to suppress noise and being able to evaluate the effective diffusive properties of the ionic species in the hydrogel. Following fitting, each conductive salt's diffusivity (D) and charge transfer resistance (R_{ct}) were determined from each sample. Results are reported in Fig. 3d, Fig. S14 and Table S2. As expected, the diffusivity strongly depends on the electrolyte species. LiCl and NaCl exhibit significantly higher effective diffusivities than KCl and RbCl. Since these values correspond to the effective diffusivity of the electrolyte, they cannot be directly interpreted as the mobility of individual ions. Rather than being governed only by ionic size, in fact, the transport process is strongly affected by ion-polymer interactions within the hydrogel network, as discussed previously. In particular, Li^+ ions experience the strongest confinement within the hydrogel matrix, leading to a larger mobility asymmetry relative to Cl^- ions. Under mechanical deformation, this asymmetry promotes greater charge separation and consequently enhances the piezoionic voltage and current generation, in agreement with the experimental results obtained for LiCl-based hydrogels. Following the trend in diffusivities, the other electrolytes cause lower piezoionic effect, also induced by a higher viscosity and stiffer mechanical properties of the hydrogel. It is also interesting to examine the trend of charge transfer resistance, i.e., the resistance encountered by charges when transferring from the hydrogel to the electrode, which shows an opposite trend to that of ion diffusivity. These values help to explain why the generated current in piezoionic hydrogels containing salts different than LiCl is very low in the parallel configuration, but significantly higher in the sandwich configuration. In the parallel arrangement (Fig. 3b), the generated current is primarily governed by cation diffusivity due to the relatively large distance between electrodes. In contrast, in the sandwich configuration (Fig. 3c), the reduced electrode separation allows effective charge transfer between the hydrogel and electrodes to significantly contribute to the piezoionic current. Consequently, the LiCl sample consistently exhibits the highest current, owing to its superior ion diffusivity, whereas NaCl, KCl, and RbCl samples show enhanced currents in the sandwich configuration due to more efficient interfacial charge transfer. It is worth noting that specific capacitive effect on the piezoionic response on the different hydrogels can be neglected, since similar capacitances (of the order of 20–30 nF) were obtained for all the samples.

A static force test further confirmed that differences in ion mobility inside the hydrogel significantly affect the piezoionic electrical output. The sandwich-shaped samples were subjected to compression with a constant force sustained for 4 min. The test was performed on the samples with different chloride salts and the blank one, to determine how long the piezoionic current can persist in a sample under a constant deformation. The normalized generated electrical current results are presented in Fig. 3e. As expected, the current is generated upon application of compressive force, resulting from the difference in ion species flux within the hydrogel. When the electrolyte flow subsides, the transient charge separation decays, leading to an exponential decrease in current due to charge recombination. The time constant of the exponential decay returns information on the ion species mobility. As shown in the inset of Fig. 3e, the constant time tends to increase with the radius of the cation. LiCl salt has the smallest time constant, which means that in the sample containing this kind of compound the ion mobility is higher and the charge separation recombines quickly, followed by NaCl and KCl, and finally RbCl, which is the one that takes the longest time to return to equilibrium due to its lower mobility. The longer time measured for the blank samples can be related to the low charge density related to dissociation of acrylic acid, whose charges are also hindered by intermolecular bonds.

The same analysis on the role of ion mobility was conducted in tensile stress test. The dumbbell-shaped samples prepared with different chloride salts were subjected to tensile testing using a speed of 200 mm min^{-1} with deformations from 0% to 20%, 50% and 80%. The signal is much more defined when the material is elongated with respect to compression, as seen in Fig. 3f. As already observed for compressive test, the piezoionic current and voltage outputs during the tensile test are dependent on the difference in mobility between cation and anion. The higher electrical outcomes are observed for LiCl and the lower ones for RbCl, as evidenced in Fig. 3f and in the current and voltage results obtained with different tensile strains presented in Fig. S15. Responses steadily increase when strain rises between 20% and 50% but significantly drop when exceeds 50% of deformation as the ionic path length increases excessively.

A fundamental application of piezoionic phenomenon reside in strain and pressure sensors, therefore the analysis of the lowest sensitivity to deformation of the material is a crucial figure of merit. The sensor's performance under small strains was studied using cyclic compressions between 0.1% and 15% of strain, with an application frequency of 2 Hz. This test has been performed using a Dynamic Mechanical Thermal Analysis (DMTA) machine to generate the mechanical stimulus coupled with the electrometer to register the piezoionic electrical output. Piezoionic current and voltage results are shown in Fig. 3g and h, respectively, evidencing a growth of the electrical output with the increasing of the mechanical deformations. In both cases, the electrical signals are fully tracked, allowing detection in the nA and μV range also of the tiniest compression. This ability to recognize very small strains is a critical feature for flexible and soft sensors, that can be used for a wide

variety of applications such as biological signals monitoring, muscle movements, robotics, and wearables. Finally, the behavior of piezoionic current was investigated at different temperatures, while cyclically compressing the sample at 1% strain with a frequency of 1 Hz (Fig. 3i). Observing DMTA curves (Fig. S16a) it is evident that the transition between the rubbery state and the glassy state in the polymer network begins below 5 °C, as it emerges by the increase of E', reaching the glassy plateau below −10 °C. This can be partially related to the freezing of the water trapped in the polymeric network (see endothermic peaks in DSC curves in Fig. S16b), with ice melting at −7.5 °C. Noteworthy, the presence of the salt has also an antifreezing effect, with icing of the water trapped decrease of more than 10 degrees (Fig. S16b). In any case, this transition is reflected in the ion mobility, which is consistently reduced in glassy polymers, leading to very low current output. As the temperature increases, the electrical response increases, as expected [52]. In parallel, the same consideration can be taken by analyzing voltage output (Fig. S16c). Besides the type of salt and room temperature, variations in salt concentration and relative humidity may influence the piezoionic response. The present measurements were performed using 1 M salt concentration under ambient laboratory conditions. Systematic testing at different salt concentrations at controlled relative humidity levels will be required in future studies to further optimize the performance of the sensor under different environmental conditions.

2.3. 3D printed piezoionic devices

The characterization of flat samples evidenced that hydrogels with LiCl tend to have the best performance because of the larger ionic mobility difference between cations and anions. Therefore, this composition was used to investigate the role of device geometry on piezoionic effect by 3D printing models, with complex shapes. Consequently, the printability of the ink was evaluated through real-time photo-rheology, where it assessed that the polymerization occurs

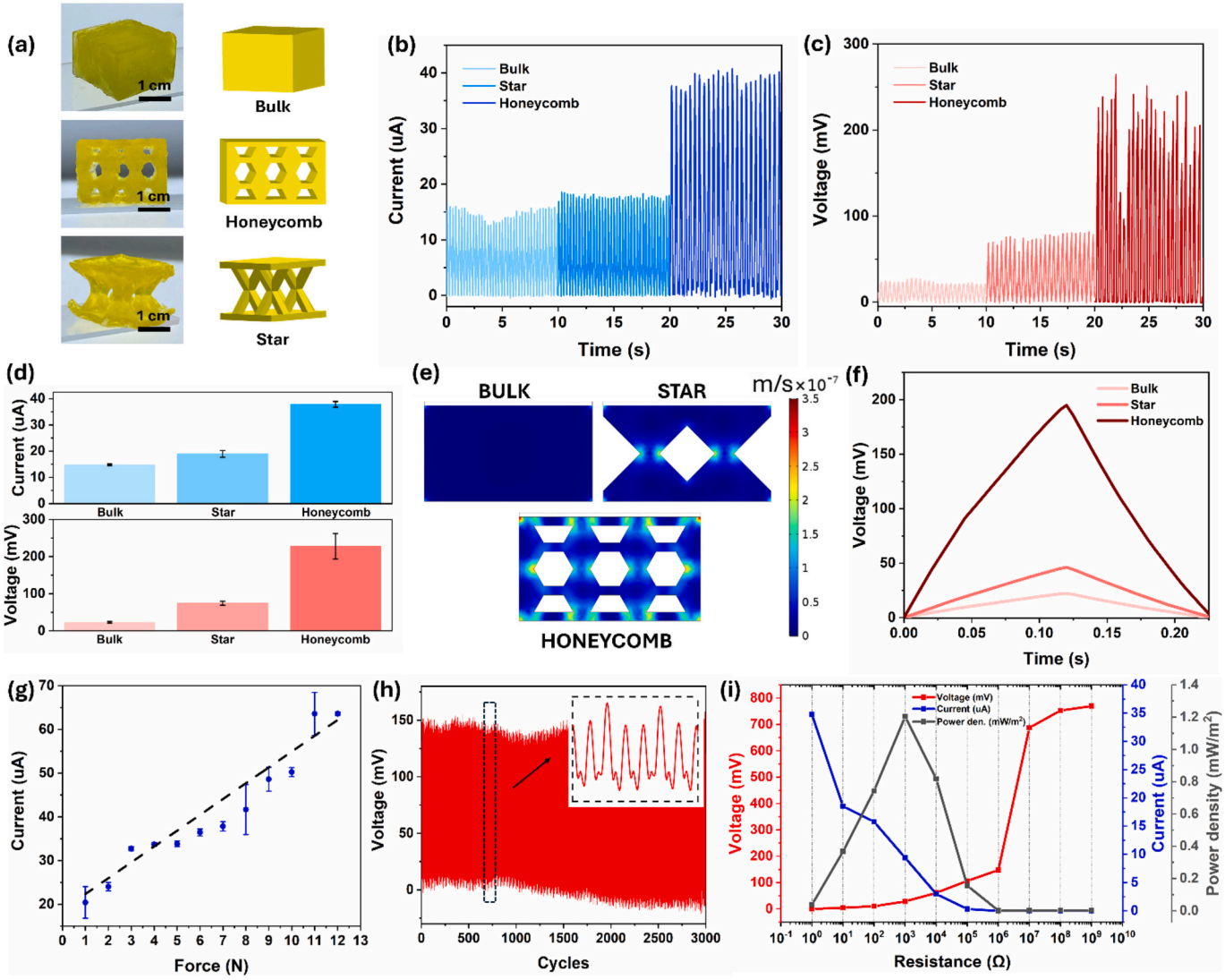


Fig. 4. 3D-printed piezoionic hydrogel pieces. a) Printed compression samples (bulk, honeycomb, stars) and their STL models. The samples have a thickness of 1 cm and an area of 1.5 cm^2. b) Electrical current and c) voltage output of 3D specimens subjected to a cyclic compression test (frequency of 4 Hz and force of 10 N) and d) bar chart of the results. Error bars represent the standard deviation of peak values over 10 consecutive cycles. e) Simulated Darcy flow velocity in the 3D printed piezoionic samples under a force of 10 N. The color bar is the same for all the simulations. f) Simulated piezoionic voltage output under a compression with peak force of 10 N and frequency of 4 Hz. g) Evolution of the current output of a honeycomb 3D specimen as function of the force in a range from 1 N to 12 N. Error bars refer to the standard deviation of peak values over 10 consecutive cycles. h) Stability performance under mechanical stimulus of a honeycomb sample. The inset reports a zoom over some mechanical cycles. i) Impedance test results: output voltage, current, and electrical power density of a honeycomb piece under different load resistances in a range from 1 Ω to 1 GΩ.

around 10 s after turning on the UV light (Fig. S17). This range is suitable for vat polymerization [53] and consequently, structures with bulk, honeycomb and star-shaped designs were printed (Fig. 4a). Printing parameters were optimized via multiple trials, final values are reported in the experimental section.

Likewise flat specimens, these 3D parts were tested under dynamic mechanical stimulation. As shown in Fig. 4b and c 3D components show higher electrical values for both voltage and current outputs than those obtained with flat samples. Fig. 4d shows the bar diagrams of the current and voltage corresponding to the average of 10 deformation cycles under a compressive force of 10 N. In particular, the honeycomb structure exhibits a remarkable current output of 37.848 μA and a voltage of 227.6 mV, corresponding to a fourfold increase in current and an order-of-magnitude enhancement in voltage compared to the bulk sample. The 3D-printed star geometry also enhances the piezoionic response relative to the bulk material, yielding more than twice the voltage output, although its performance remains below that of the honeycomb structure. The enhancement in piezoionic performance can be attributed to the higher mechanical deformation of the complex architectures, under the same applied load, compared to the bulk structure, leading to higher localized mechanical stresses. This, in turn, increases the Darcy flow velocity within the polymeric network, thereby amplifying the ionic flux and the difference between cation and anion motion. Collectively, these effects result in the observed improvement in piezoionic voltage and current. To validate this interpretation, simulations were conducted based on the theoretical framework described above. The results confirm that the Darcy flow velocity in the honeycomb structure is several times higher than in the star and bulk configurations (Fig. 4e), particularly in regions of stress concentration (Fig. S18). Using this data, the simulated piezoionic voltage output was calculated, reproducing the experimental trend and demonstrating a tenfold enhancement in performance for the honeycomb geometry (Fig. 4f). A comparison with several notable and recently reported piezoionic hydrogel-based sensors is summarized in Table S3. According to the results, the proposed device demonstrates competitive performance and stands out among other recently reported, highlighting its potential for piezoionic sensing applications and the employment of DLP 3D printing for the fabrication of complex and customized architectures.

Similar to other studies, there is a linear relationship between the increase in electrical response as the deformation force gradually rises (Fig. 4g) [54–56]. Between a force range of 1 N and 12 N, the sensor exhibits a sensitivity of 3.62 μA N^{-1}. Another important feature to implement in piezoionic devices for sensing application is the stability and repeatability in time. The stability of the device's electrical response over time was assessed using a honeycomb 3D structure. The 3D sample was continuously mechanically deformed over time. Fig. 4h presents the results, which show no mechanical fatigue of the sample or reduction in response during constant stimulation, demonstrating optimal reliability and performance.

Strain and pressure sensing are not the only application fields of piezoionic material. Since piezoionics can convert mechanical stimuli into an electrical signal, their output can be used to harvest mechanical waste energy, leading to the development of PHNGs. The honeycomb structure was used to evaluate the maximum electrical power generation of hydrogel. The voltage and current generated by the sample were measured under external load resistances ranging from 1 Ω to 1 GΩ. As expected, the output voltage increases with increasing load resistance, while the current decreases steadily (Fig. 4i). The maximum power density of 1.20 mW m^{-2} is reached at load resistances near 1 kΩ. This maximum output power results from impedance matching between the external load and the piezoionic nanogenerator, which exhibits an internal resistance in the kilo-ohm range. Although the power density achieved here is relatively modest compared with that typically reported for piezoelectric and triboelectric nanogenerators (approximately 0.1–10 W m^{-2}, with optimized triboelectric systems reaching instantaneous peak values of several hundred W m^{-2}) [57–59] it is important to emphasize that devices exploiting the piezoionic effect are still at an early stage of development. At present, their relatively low power density limits their applicability as general-purpose energy harvesters and makes them more suitable for low-power, self-powered sensing. Nevertheless, substantial improvements may be achieved through further optimization of material composition, ion selectivity, electrode interfaces and device architecture. Notably, compared to other nanogenerator technologies, our piezoionic hydrogel nanogenerator (PHNG) delivers an exceptionally high charge density, on the order of 10 μC cm^{-2}. This value exceeds those typically reported for piezoelectric and triboelectric systems by at least three orders of magnitude [60,61]. The inherently high charge generation capability of piezoionic systems is particularly appealing for bioelectronic and neural interface applications, where charge injections of tens of microcoulombs per square centimeter are routinely required, and maintaining low operating voltages is essential for safety [62]. However, the generated surface charge density should not be interpreted directly as electrochemical charge-injection capacity; its suitability for neural stimulation would require dedicated evaluation of electrode-interface reactions, charge-transfer efficiency, waveform characteristics and tissue-safety limits. Moreover, the intrinsic softness of the hydrogel material offers a significant advantage for energy harvesting from human motion, as it minimizes interference with natural body movements and enhances wearer comfort during use.

2.4. Applications for wearable sensing and energy harvesting

The previously reported results led to the implementation of several piezoionic PVA/AAc/LiCl samples in various proof-of-concept applications to illustrate and evaluate the hydrogel's performance as a potential biomedical sensor and energy harvester. First, the hydrogel was implemented to record movements of different parts of the body. In these analyses, the generated voltage or current under mechanical stimulation were recorded to demonstrate that the piezoionic signals can be used for wearable sensing applications. Initially, the vocal cord vibrations during laughter were tracked using a strip-shaped sensor. The sample was placed on the throat. As can be seen in Fig. 5a, each of the current spikes corresponds to a single laugh, confirming the sensor's ability to record this tiny signal. Then, the same sensor was used to monitor the flexion of the index finger at different movement frequencies (Fig. 5b). In addition, the electrical response of the fingers' extrinsic muscles, located on the forearm, was successfully monitored during the hand opening and closing movements. As shown in Fig. 5c, the current rises during hand closure due to skin deformation caused by muscle contraction, then decreases as the hand is opened. The sensor was then positioned on the wrist to assess the capability of heart rate detection. To verify the effective monitoring performance, a piezoionic sensor was also placed on the front part of the forearm where the pulse wave is absent, while no external movements were performed. The results are illustrated in Fig. 5d. When the sensor is placed on the forearm, the current is noisier because the artery, from which pulse deformation derives, is situated deeper beneath the skin surface, while when it is placed on the wrist, a clearer pulse waveform is obtained, and the pressure generated by each heartbeat can be sensed. Fig. 5e shows a zoom of the pulse waveform obtained during the test where the characteristic points are visible, confirming its capability to track heart rate. The sensor displayed promising performances also for gait analysis. In this case the device was placed in the sole of the shoe (Fig. S19) and the results registered for both current and voltage are presented in Fig. 5f, demonstrating the sensor's ability to detect both normal and fast walking (see Supplementary Video). Further integration of these materials with soft and stretchable electrodes could improve the conformability of the sensors to the human body, thereby enhancing skin–sensor contact and facilitating reliable detection of biometric signals. To demonstrate the energy harvesting ability of the device, the hydrogel was applied to charge a 1 μF capacitor. A 3D-printed honeycomb-shaped sample was subjected to

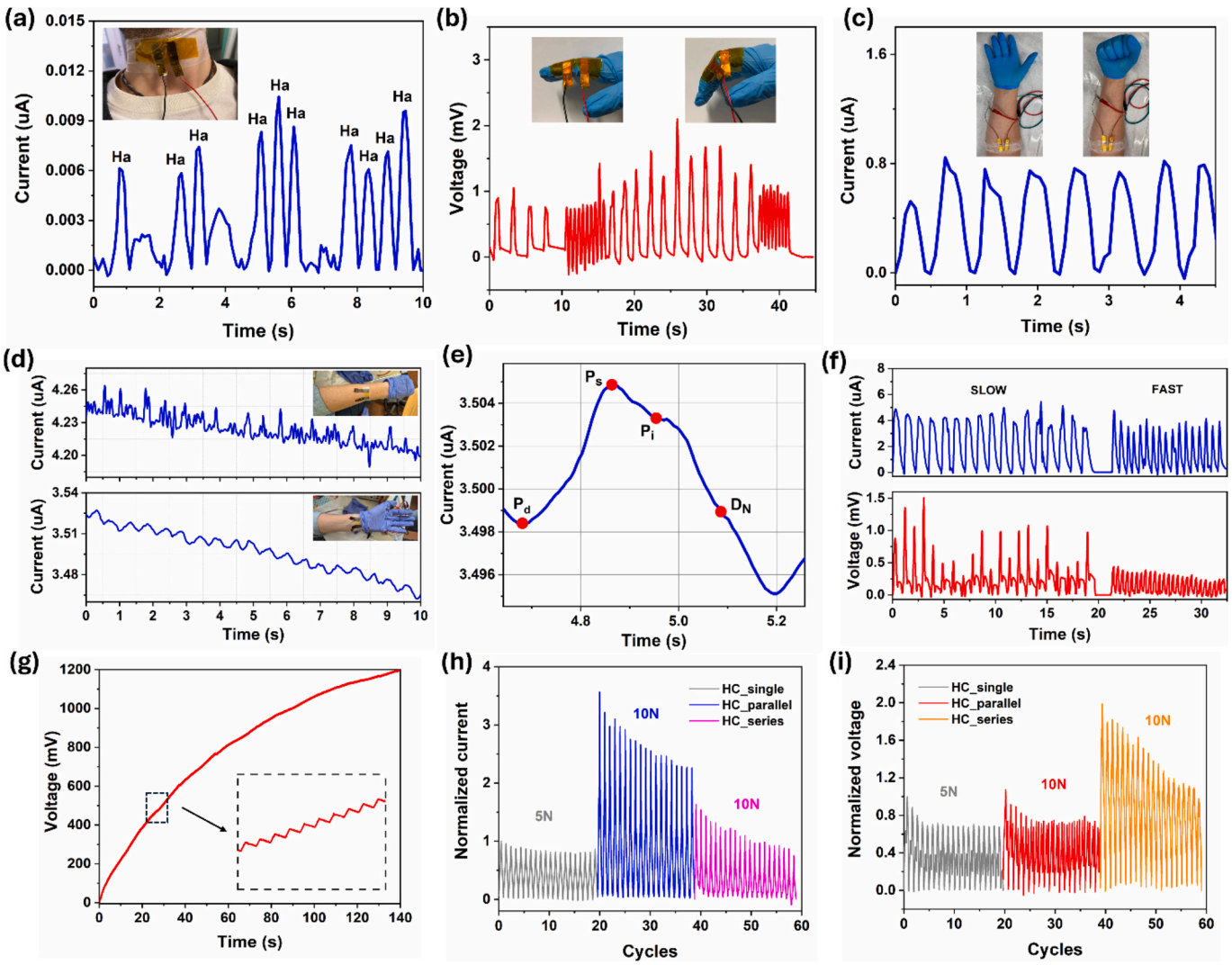


Fig. 5. Performances of flat and 3D piezoionic hydrogel samples. a) Recognition of vocal cord movement during laughter. b) Finger bending monitoring with different speeds movements. c) Current response to hand opening and closing. d) Heart rate sensed on the forearm (top) and on the wrist (bottom). e) Zoom of the pulse waveform with the corresponding diastolic pressure *(Pd)*, systolic pressure *(Ps)*, inflection point *(Pi)* and the dicrotic notch *(Dn)*. f) Recording of the electric current (top) and voltage (bottom) output during a walk at different speeds. g) Charging of 1 μF capacitor for 140 s during a constant mechanical deformation of a honeycomb sample. Some charging steps are shown in the inset. h) The improvement of instantaneous current by connecting in series two piezoionic 3D printed devices. i) The improvement of instantaneous voltage by connecting in series two piezoionic 3D printed devices.

periodic compressive deformations with the shaker. The assembly was then connected to a rectifier circuit and the capacitor. Fig. 5g shows that the capacitor is charged to almost 1 V in around 2 min. Each mechanical deformation generates about 20 mV of storage energy that later can be used for other purposes. In addition, multiple 3D printed piezoionic honeycomb structures were connected either in series or in parallel to obtain higher electrical outputs for energy harvesting purposes. A polydimethylsyloxane (PDMS) separator was used to enclose the piezoionic devices, helping to keep the correct position during the multiple compression loads (Fig. S20a). The devices were then placed in the compression fixtures, and a cyclic compressive load was applied (Fig. S20b). The measured voltages and currents were normalized with respect to the values generated by a single honeycomb structure, tested applying a 5 N load (Fig. 5h-i). Subsequently, parallel and series configurations with two 3D printed honeycomb structures of identical dimensions were assembled as shown in Fig. S20c. The dual-harvester configuration was evaluated under a 10 N load to ensure comparable pressure conditions with the single-cell harvester. As shown in Fig. 5i, the peak output voltage nearly doubled when the two honeycomb structures were connected in series. Assuming ideal voltage generator behavior, the total potential difference across the terminals is expected to double in series connection. Conversely, when connected in parallel, the output voltage remained nearly constant, while the generated current approximately doubled relative to the single-cell configuration. Minor deviations from ideal behavior can be attributed to surface irregularities and slight geometric differences between the two samples. These results demonstrate that piezoionic devices can be effectively combined in series or parallel configurations to selectively enhance voltage or current output, respectively, consistently with the behavior of other common energy harvesters. Overall, this confirms the potential of the developed material as a tactile energy-harvesting sensor, capable of converting various human body movements into storable electrical energy.

3. Conclusions

This work provides a comprehensive analysis of the piezoionic phenomenon, elucidating how ion-mobility asymmetry and device architecture govern the electrical response of ionic hydrogels. Different hydrogel-electrodes configurations were investigated together with the

piezoionic response to both compressive and tensile mechanical stimuli. Leveraging the 3D-printing capability of the photocurable, self-healing hydrogel, we demonstrate that complex geometries can be engineered to concentrate local mechanical stress, thereby markedly amplifying the piezoionic output. We further show that the material retains its electromechanical functionality after damage through autonomous self-healing and that tensile deformation can also be exploited to generate measurable electrical signals.

Together, these findings advance the fundamental understanding of piezoionic mechanisms and establish new design principles for high-performance ionotronic systems. Building on these insights, we demonstrate that the material can serve as a functional platform for the development of self-powered wearable biometric sensors. Further integration with soft and stretchable electrodes, such as liquid metals or conductive polymers, in place of rigid metallic films could enable the development of fully flexible and wearable sensing systems suitable for practical applications. We further demonstrate that the electrical energy generated under mechanical stimulation can be harvested using a piezoionic hydrogel nanogenerator (PHNG). Although further optimization is required for its energy-harvesting performance to approach that of established piezoelectric and triboelectric nanogenerators, these results demonstrate the potential of piezoionic hydrogels as soft mechanical-energy harvesters. Further optimization of the ion concentration and polymer-network composition could enhance the mobility contrast between cations and anions, thereby increasing the piezoionic output. Additional performance gains could be achieved by exploring alternative device geometries and improving integration with the electrodes and power-management electronics. These results and possible improvements open promising avenues for next-generation soft robotics, flexible electronics, and sustainable energy-harvesting technologies.

4. Materials and methods

4.1. Materials

For the main composition of the hydrogel were used deionized water, acrylic acid (AAc), poly (vinyl alcohol) (PVA) (MW 89000–98,000 Da, 99 + % hydrolyzed) and poly (ethylene glycol diacrylate) (PEGDA) (MW 575). Water-soluble diphenyl(2,4,6-trimethylbenzoyl) phosphine oxide-based nanoparticle photoinitiator containing ionic surfactant (TPO-SDS) was employed as a polymerization activator, while tartrazine was utilized to form an organic-water soluble dye to improve the printing resolution and to avoid polymerization over the exposed areas [27,28]. For the analysis of ionic mobility, lithium chloride (LiCl), sodium chloride (NaCl), potassium chloride (KCl), and rubidium chloride (RbCl) were added to different formulations. The molecular weight of the salts is presented in Table S4. All the components were purchased from Sigma Aldrich (USA). Polyimide-copper electrodes were used for electrical characterization. To prepare the hydrogel, the salt was dissolved at a concentration of 1 M in deionized water (16 mL) using a magnetic stirrer. The formulation was cooled down to 4 °C in an ice bath, and then the PVA (4 g) was added and dissolved in the water solution while stirring at 150 rpm for 45 min. At this point, a white, homogeneous solution was obtained. Afterwards, the flask was immersed into a silicone oil bath at 90 °C while the stirring speed was reduced to 100 rpm for 60 min. Once the solution became transparent, the content was allowed to cool to room temperature. The formulation was transferred to a container and then the AAc (5 g), PEGDA (50 mg), dye (1.5 mg) and TPO photoinitiator (75 mg) were added. Finally, the entire formulation is mixed using a centrifuge (THINKY mixer AR-100) at 2000 rpm for 5 min. In addition, a defoaming was carried out for 5 min to obtain a completely homogeneous solution without air bubbles.

4.2. Piezoionic devices assembly

To carry out the electromechanical characterization of the sensor under different parameters, various configurations that matched the features of the machines were designed. Two specific types of flat models were used to evaluate how the distance between the electrodes can affect the electrical response. The first model was built in a parallel arrangement, using the hydrogel as an elongated rectangular band (3 × 1.5 × 0.15 cm), to which two electrodes were affixed at the extreme sides, spaced apart by 1 cm. The sandwich arrangement was the second model, inserting flat samples with a 15 × 10 mm^2 area and 1.5 mm of thickness within two strip copper electrodes. Both configurations were employed to analyze cyclic deformations during compression and vibration tests. Finally, dog-bone shaped samples of 4 cm length and 1.5 mm thickness were assessed for tensile tests. A study with bare copper foils and carbon-coated foils was carried out in flat sandwich samples with LiCl inside. All samples were subjected to a constant mechanical deformation of 10 N at a frequency of 2.5 Hz (Fig. S1). Although the use of carbon electrodes allows for greater stability and better surface area with respect to the electrolyte, in this case, as shown by the results mentioned above, the possible effects of interfacial charge transfer are negligible as the responses remain relatively unchanged with or without the coating.

4.3. Electrical, mechanical and physical characterization

Tensile and compression tests were performed with the Tensile Test Z5 machine and were controlled through the THSSD program. A high impedance electrometer (Keithley 2400, Tektronix) was used to track voltage and current electrical responses during each test. In the case of compression with sandwich-like sensors, two strips of conductive tape were used as electrodes that were adhered to the upper and lower grasp of the machine, and the sample was arranged between both to exert pressure on it. Parallel samples were glued to a support on the lower grasp of the machine using a biadhesive and the electrodes were clamped to multimeter.

Dynamic testing was carried out using a mechanical shaker (TV51110, Tira System) driven in a closed loop by a controller unit (VR 9500, Vibration Research) and a power amplifier (BAA 120, Tira System). A metal bar that was movable by a knob was fitted to exert pressure on the material and conduct the electromechanical tests. To determine the strength and acceleration with which the bar would strike the sample, a force sensor and an accelerometer were mounted to the shaker. The vibrating system was controlled by the VibrationVIEW program, in which it was possible to set the displacement of the shaker and the vibrating frequency, as well as to monitor the force and acceleration exerted on the sample. The Keithley 6517B electrometer (Tektronix) was used to track the behaviors of electrical signals. Both parallel and sandwich samples were bonded with a double-sided adhesive tape to the bottom of the metal bar so the force sensor could encounter the sensor electrodes. Data acquisition and parameter settings were executed using LabView. Samples containing each of the salts as well as a reference sample without salt were utilized for every test.

The viscosities of the formulations varying the salt types were analyzed through rheological measurements, using an Anton Paar Physica MCR 302 rheometer in 25 mm diameter parallel plate mode. A gap of 0.5 mm between plates was set and rotation shear ramp tests between 0.01 × 1 and 1000 × 1 s^{-1} were carried out. The photopolymerization of the ink was evaluated by real-time photorheology test. In this analysis, a 25 mm diameter parallel plate mode (gap of 0.2 mm) with a quartz lower plate was used to measure the variation of the polymer viscoelastic properties upon light irradiation. The light source used was a Hamamatsu LC8 lamp, equipped with a light guide (UV light, intensity 25 mW cm^{-2}). The light was turned on after 60 s to allow the stabilization of the system. All the rheological tests were performed at 25 °C. The test was performed at a constant strain amplitude of 1% and a constant shear frequency of 1 Hz.

EIS test was performed on a sensor with a parallel configuration with very small electrodes separated by 10 μm, to study the some of the

electrochemical properties of the material, specifically, the interaction of the salts contained within the hydrogel with the polyimide-copper electrodes. The specimen was subjected to an alternating voltage of 50 mV as a function of frequency, varied in the range 100 kHz – 1 mHz, using a Multi Autolab/M101 (Metrohm) electrochemical working station. An impedance measurement was executed and then the results were fitted based on an experimental circuit model, reported in the inset of Fig. S14, composed by a series resistance R_s, a high-frequency parallel between transport resistance R_t and capacitance C_t, a low frequency parallel composed by the charge transfer resistance R_{ct} and the double layer capacitance C_{dl}, and a Finite Length Warburg element Z_{diff} accounting for the diffusion, given by

$$Z_{diff} = \frac{R_{diff}}{\sqrt{j\omega}} coth\left(\delta\sqrt{\frac{j\omega}{D}}\right) \quad (4)$$

where R_{diff} is the diffusion resistance and δ is the gap between electrodes [63]. Afterwards, the diffusivity and charge transfer resistance parameters of each of the conductive salts were extracted.

DMTA experiments were performed using an Anton Paar MCR 703, coupled with voltage and current responses tracking. Parallelepiped-shaped samples (nominal dimensions of 15 × 10 × 10 mm^3) were subjected to cyclic compressive testing at room temperature with a constant application frequency of 2 Hz. Compressive deformations of 0.1%, 0.3%, 0.5%, 0.8%, 1%, 5%, 10% and 15% were applied sequentially. Moreover, to evaluate the temperature dependence of piezoionic effect, additional cyclic compressive test (1% of deformation, 1 Hz as frequency) was performed increasing the temperature from −20 °C to 43 °C, with a heating rate of 2 °C $minL^{-1}$ in a sample of 3 mm of thickness.

DSC (Differential Scanning Calorimetry) were performed with a Mettler Toledo DSC 3 equipment. Cooling and heating processes were carried out with a 2 °C $minL^{-1}$ rate and in inert atmosphere (N_2 flux = 50 mL $minL^{-1}$).

4.4. 3D printing

A commercial 3D Digital Light Processing (DLP) printer (Asiga MAX X UV385) with a light emission wavelength centered at 385 nm and nominal resolution of 27 × 27 μm^2 was employed to study the piezoionic phenomenon samples with different structures. The first 4 burn-in layers were irradiated with a light intensity of 32 mW cm^{-2} for 8 s while the following slices were exposed for 6 s with a light intensity of 30 mW cm^{-2}. In addition, all the models were printed with a separation velocity of 2 mm s^{-1} and an approach velocity of 4.3 mm s^{-1} to prevent as many viscosity defects as possible on the samples. To avoid water evaporation during the printing process it was necessary to use a water vapor flux (30 mL h^{-1}) supplied by TaoTronics TTAH002 [28]. To get rid of any remaining unreacted resin, samples were submerged in ethanol for 3 min while being smoothly sonicated (Sonorex Digiplus, Bandelin). Finally, the models were subjected to a post-curing procedure for 3 further minutes under UV light (Robofactory UV oven).

4.5. Finite element analysis

Finite Element Analysis (FEA) was performed using COMSOL Multiphysics 5.3. The model was developed to compute mechanical stress distribution in the hydrogel samples using the Solid Mechanics module, and subsequently solved iteratively by coupling the Poroelasticity, Transport of Diluted Species, and Electrostatics modules. Models were constructed for the parallel, sandwich, and 3D-printed configurations, employing the actual sample dimensions, as well as the elastic modulus and ionic mobility values obtained from mechanical testing and EIS, respectively. The bottom surface of each model was assigned a fixed boundary condition, while all remaining surfaces were allowed to deform freely. The parameters used in the simulations are summarized in Table S5 and were selected based on experimental results, relevant literature [16,34], and comparison with the measured data.

CRediT authorship contribution statement

Maria Jose Arias Belduque: Writing – original draft, Visualization, Validation, Investigation, Formal analysis, Data curation. **Giorgio Mogli:** Writing – original draft, Visualization, Formal analysis, Data curation. **Adriano Sacco:** Writing – review & editing, Investigation, Conceptualization. **Ignazio Roppolo:** Writing – review & editing, Validation, Methodology, Conceptualization. **Stefano Stassi:** Writing – review & editing, Supervision, Methodology, Funding acquisition, Conceptualization.

Declaration of competing interest

The authors declare that they have no known competing financial interests or personal relationships that could have appeared to influence the work reported in this paper.

Acknowledgement

This research was supported by the Ministero dell'Università e della Ricerca (MUR), through PRIN 2022 - PASSO Prot. 20222TKNRJ grant and is part of the project PNRR-NGEU which has received funding from the MUR – DM 629/2024. This work was developed in the frame of MICS (Made in Italy – Circular and Sustainable) Extended Partnership and received funding from the European Union Next-GenerationEU (PIANO NAZIONALE DI RIPRESA E RESILIENZA (PNRR) – MISSIONE 4 COMPONENTE 2, INVESTIMENTO 1.3 – D.D. 1551.11-10-2022, PE00000004). This manuscript reflects only the authors' views and opinions, neither the European Union nor the European Commission can be considered responsible for them.

Appendix A. Supplementary data

Supplementary data to this article can be found online at https://doi.org/10.1016/j.cej.2026.182105.

Data availability

Data will be made available on request.

References

[1] T.-D. Nguyen, J.S. Lee, Recent development of flexible tactile sensors and their applications, Sensors 22 (50) (2022).
[2] Y. Al-Handarish, et al., A survey of tactile-sensing systems and their applications in biomedical engineering, Adv. Mater. Sci. Eng. 2020 (2020) 4047937.
[3] S.S. Robinson, et al., Integrated soft sensors and elastomeric actuators for tactile machines with kinesthetic sense, Extreme Mech. Lett. 5 (2015) 47–53.
[4] Z. Zhao, et al., Recent development of self-powered tactile sensors based on ionic hydrogels, Gels 9 (257) (2023).
[5] S. Li, et al., Physical sensors for skin-inspired electronics, InfoMat 2 (2020) 184–211.
[6] J. Qu, et al., Recent progress in advanced tactile sensing technologies for soft grippers, Adv. Funct. Mater. 33 (2023) 2306249.
[7] S. Chun, Y. Kim, H.-S. Oh, G. Bae, W. Park, A highly sensitive pressure sensor using a double-layered graphene structure for tactile sensing, Nanoscale 7 (2015) 11652–11659.
[8] B. Herren, et al., PDMS Sponges with Embedded Carbon Nanotubes as Piezoresistive Sensors for Human Motion Detection, Nanomaterials 11 (2021).
[9] S.G. Yoon, B.J. Park, S.T. Chang, Highly sensitive piezocapacitive sensor for detecting static and dynamic pressure using ion-gel thin films and conductive elastomeric composites, ACS Appl. Mater. Interfaces 9 (2017) 36206–36219.
[10] S. Baek, et al., Flexible piezocapacitive sensors based on wrinkled microstructures: Toward low-cost fabrication of pressure sensors over large areas, RSC Adv. 7 (2017) 39420–39426.
[11] N.A.-O. Kamel, Bio-piezoelectricity: fundamentals and applications in tissue engineering and regenerative medicine, Biophys. Rev. 14 (2022) 717–733.
[12] G. Zhao, et al., Transparent and stretchable triboelectric nanogenerator for self-powered tactile sensing, Nano Energy 59 (2019) 302–310.

[13] H. Lei, et al., Self-assembled porous-reinforcement microstructure-based flexible triboelectric patch for remote healthcare, Nano Micro Lett. 15 (2023) 109.
[14] M. Sarwar, et al., Proc. SPIE 9430, Electroactive Polymer Actuators and Devices (EAPAD) 2015, University of Wollongong, 2015.
[15] D. Ho, The piezoionic effect: biomimetic transduction mechanism for sensing, actuation, interface, and energy harvesting 11 (2024) e202300268.
[16] Y. Dobashi, et al., Piezoionic mechanoreceptors: force-induced current generation in hydrogels, Science 376 (2022) 502–507.
[17] Z. Chen, Y. Wang, Ionic skin: from imitating natural skin to beyond, Industrial Chemistry & Materials 1 (2023) 224–239.
[18] G. Di Pasquale, S. Graziani, A. Latteri, A. Pollicino, C. Trigona, Poly (ε-caprolactone)–ionic liquid composite as piezoionic mechanical sensor, Appl. Sci. 14 (2024) 1085.
[19] Y. Fang, et al., Ultrasensitive multi-degree-of-freedom piezoionic sensor via synergistic hydrogel-ion interactions, Nat. Commun. 17 (893) (2025).
[20] H. Lu, N. Zhang, M. Ma, Electroconductive hydrogels for biomedical applications, Wiley Interdiscip. Rev. Nanomed. Nanobiotechnol. 11 (2019) e1568.
[21] T.-C. Ho, et al., Hydrogels: properties and applications in biomedicine, Molecules 27 (2022) 2902.
[22] K. Saha, A. Chatterjee, A. Das, A. Ghorai, U. Jeong, Self-powered ionic tactile sensors, J. Mater. Chem. C 11 (2023) 7920–7936.
[23] D. Cafiso, S. Lantean, C.F. Pirri, L. Beccai, Soft mechanosensing via 3D printing: a review 5 (2023) 2200373.
[24] Y. Yu, et al., Highly conductive, stable, and self-healing MXene-based hydrogel sensor via a controlled assembly of polydopamine and cellulose nanocrystal, Energy Environ. Mater. 9 (2026) e70105.
[25] B. Wan, et al., Water-dispersible and stable polydopamine coated cellulose nanocrystal-MXene composites for high transparent, adhesive and conductive hydrogels, Carbohydr. Polym. 314 (2023) 120929.
[26] J. Xu, Q. Li, D. Ho, A universal framework for determining the effect of operating parameters on piezoionic voltage generation, Mater. Horiz. 11 (2024) 5709–5721.
[27] M. Caprioli, et al., 3D-printed self-healing hydrogels via digital light processing, Nat. Commun. 12 (2021) 2462.
[28] G. Mogli, et al., Self-powered integrated tactile sensing system based on ultrastretchable, self-healing and 3D printable ionic conductive hydrogel, Adv. Funct. Mater. 34 (2024).
[29] Y. Liu, et al., Self-powered piezoionic strain sensor toward the monitoring of human activities, Small 12 (2016) 5074–5080.
[30] F. Li, X. Cai, G. Liu, H. Xu, W. Chen, Piezoionic SnSe nanosheets-double network hydrogel for self-powered strain sensing and energy harvesting 33 (2023) 2300701.
[31] J. Zhou, X. Lu, Y. Wang, J. Shi, Molecular dynamics study on ionic hydration, Fluid Phase Equilib. 194-197 (2002) 257–270.
[32] L. Li, et al., A d33 piezoionic hydrogel with bioinspired multi-gradient structure for enhanced mechano-iontronic transduction, Nano Energy 133 (2025) 110477.
[33] A. Adjaoud, et al., Piezoionic sensors based on formulated PEDOT:PSS and Aquivion® for ionic polymer–polymer composites, Smart Mater. Struct. 30 (2021) 105027.
[34] S. Wang, T. Yang, D. Zhang, Q. Hua, Y. Zhao, Unveiling gating behavior in piezoionic effect: toward neuromimetic tactile sensing, Adv. Mater. 36 (2024) 2405391.
[35] Y. Ouyang, et al., Mechano-driven neuromimetic logic gates established by geometrically asymmetric hydrogel iontronics, Small 21 (2025) 2409998.
[36] Z. Zhao, Y. Dai, S.X. Dou, J. Liang, Flexible nanogenerators for wearable electronic applications based on piezoelectric materials, Materials Today Energy 20 (2021) 100690.
[37] Z. Jin, F. Zhao, Y. Lei, Y.-C. Wang, Hydrogel-based triboelectric devices for energy-harvesting and wearable sensing applications, Nano Energy 95 (2022) 106988.
[38] L.E. Millon, C.J. Oates, W. Wan, Compression properties of polyvinyl alcohol – bacterial cellulose nanocomposite, J Biomed Mater Res B Appl Biomater 90B (2009) 922–929.
[39] G. Abdul-Hussain, W. Holderbaum, T. Theodoridis, G. Wei, Modified nonlinear hysteresis approach for a tactile sensor, Sensors (Basel, Switzerland) 23 (2023) 7293.
[40] A. Oliveri, M. Maselli, M. Lodi, M. Storace, M. Cianchetti, Model-based compensation of rate-dependent hysteresis in a piezoresistive strain sensor, IEEE Trans. Ind. Electron. 66 (2019) 8205–8213.
[41] D. Kim, et al., Review of machine learning methods in soft robotics, PLoS One 16 (2021) e0246102.
[42] O. Chaudhuri, Viscoelastic hydrogels for 3D cell culture, Biomater. Sci. 5 (2017) 1480–1490.
[43] A.D. Drozdov, J. de Claville Christiansen, Tuning the viscoelastic response of hydrogel scaffolds with covalent and dynamic bonds, J. Mech. Behav. Biomed. Mater. 130 (2022) 105179.
[44] J. Smith-Jones, et al., 3D printed modular piezoionic sensors using dynamic covalent bonds, RSC Applied Polymers 2 (2024) 434–443.
[45] I. Roppolo, M. Caprioli, C.F. Pirri, S. Magdassi, 3D printing of self-healing materials, Adv. Mater. 36 (2024) 2305537.
[46] W. Zhao, D. Zhang, Y. Yang, C. Du, B. Zhang, A fast self-healing multifunctional polyvinyl alcohol nano-organic composite hydrogel as a building block for highly sensitive strain/pressure sensors, J. Mater. Chem. A 9 (2021) 22082–22094.
[47] P. Sacco, et al., Ionic strength impacts the physical properties of agarose hydrogels, Gels 10 (94) (2024).
[48] S. Lu, et al., Effects of different salt ions on the structure and rheological behavior of sulfated cellulose nanocrystal hydrogel, Food Hydrocoll. 151 (2024) 109799.
[49] M. Watase, K. Nishinari, Effect of alkali metal ions on the rheological properties of κ-carrageenan and agarose gels, J. Texture Stud. 12 (1981) 427–445.
[50] Y. Sui, et al., Effect of alkali pretreatment on paramylon hydrogel: Structure, rheology, and formation mechanism, Carbohydr. Polym. Technol. Appl. 13 (2026) 101102.
[51] M. Masiak, W. Hyk, Z. Stojek, M.J.T. Ciszkowska, Structural changes of polyacids initiated by their neutralization with various alkali metal hydroxides. Diffusion studies in poly(acrylic acid)s, J. Phys. Chem. B 111 (38) (2007) 11194–11200.
[52] G. Mogli, I. Roppolo, A. Chiappone, S. Stassi, Multi-responsive 3D printable organohydrogel for the fabrication of durable and low-hysteresis flexible sensors, Appl. Mater. Today 44 (2025) 102675.
[53] L. Strohmeier, H. Frommwald, S. Schlögl, Digital light processing 3D printing of modified liquid isoprene rubber using thiol-click chemistry, RSC Adv. 10 (2020) 23607–23614.
[54] J. Odent, et al., 3D-printed stacked ionic assemblies for iontronic touch sensors, Adv. Funct. Mater. 33 (2023) 2210485.
[55] W. Liu, et al., Cationic chitosan enables eutectogels with high ionic conductivity for multifunctional applications in energy harvesting and storage, Int. J. Biol. Macromol. 286 (2025) 138229.
[56] M. Biao, et al., A dual-mode wearable sensor with coupled ion and pressure sensing, Soft Science 4 (8) (2024).
[57] A. Chiappone, et al., Three-dimensional printing of triboelectric nanogenerators by digital light processing technique for mechanical energy harvesting, ACS Appl. Mater. Interfaces 15 (2023) 53974–53983.
[58] T. Cheng, J. Shao, Z.L. Wang, Triboelectric nanogenerators, Nat. Rev. Methods Primers 3 (39) (2023).
[59] C. Zhang, et al., Recent progress of wearable piezoelectric nanogenerators, ACS Appl. Electron. Mater. 3 (2021) 2449–2467.
[60] H. Fu, et al., Quantum dot hybridization of piezoelectric polymer films for non-transfer integration of flexible biomechanical energy harvesters, ACS Appl. Mater. Interfaces 14 (2022) 29934–29944.
[61] X. Pu, et al., Ultrastretchable, transparent triboelectric nanogenerator as electronic skin for biomechanical energy harvesting and tactile sensing, Sci. Adv. 3 (2017) e1700015.
[62] D.B. McCreery, W.F. Agnew, T.G.H. Yuen, L. Bullara, Charge density and charge per phase as cofactors in neural injury induced by electrical stimulation, I.E.E.E. Trans. Biomed. Eng. 37 (1990) 996–1001.
[63] A. Sacco, Electrochemical impedance spectroscopy: Fundamentals and application in dye-sensitized solar cells, Renew. Sust. Energ. Rev. 79 (2017) 814–829.